

RESEARCH

Open Access



# Human breast milk-derived exosomes attenuate lipopolysaccharide-induced activation in microglia

Oluwatomi Akinduro<sup>1†</sup>, Sanjay Kumar<sup>1†</sup>, Yuechuan Chen<sup>2†</sup>, Barbara Thomas<sup>1</sup>, Quamarul Hassan<sup>2\*</sup> and Brian Sims<sup>1\*</sup>

## Abstract

Microglia mediate the immune response in the central nervous system to many insults, including lipopolysaccharide (LPS), a bacterial endotoxin that initiates neuroinflammation in the neonatal population, especially preterm infants. The synthesis of the proinflammatory proteins CD40 and NLRP3 depends on the canonical NF- $\kappa$ B cascade as the genes encoding *CD40* and *NLRP3* are transcribed by the phosphorylated NF- $\kappa$ B p50/p65 heterodimer in LPS-induced microglia. Exosomes, which are nanosized vesicles (40–150 nm) involved in intercellular communication, are implicated in many pathophysiological processes. Human breast milk, which is rich in exosomes, plays a vital role in neonatal immune system maturation and adaptation. Activated microglia may cause brain-associated injuries or disorders; therefore, we hypothesize that human breast milk-derived exosomes (HBME) attenuate LPS-induced activation of CD40 and NLRP3 by decreasing p38 MAPK and NF- $\kappa$ B p50/p65 activation/phosphorylation downstream of TLR4 in murine microglia (BV2). Human microglia (HMC3) showed a significant decrease in p65 phosphorylation. We isolated purified HBME and characterized them using nanoparticle tracking analysis, transmission electron microscopy, fluorescence-activated cell sorting, and western blots. Analysis of microglia exposed to LPS and HBME indicated that HBME modulated the expression of signaling molecules in the canonical NF- $\kappa$ B pathway, including MyD88, I $\kappa$ B $\alpha$ , p38 MAPK, NF- $\kappa$ B p65, and their products CD40, NLRP3, and cytokines IL-1 $\beta$  and IL-10. Thus, HBMEs have great potential for attenuating the microglial response to LPS.

**Keywords** Breast milk, Exosomes, Microglia, HMC3, BV2, Neonatal neuroinflammation, Lipopolysaccharide, NF $\kappa$ B, CD40, NLRP3, IL-1 $\beta$ , IL-10

<sup>†</sup>Oluwatomi Akinduro, Sanjay Kumar and Yuechuan Chen have equally contributed as co-first authors.

\*Correspondence:

Quamarul Hassan

hassank@uab.edu

Brian Sims

bsims@peds.uab.edu

<sup>1</sup> Department of Pediatrics/Division of Neonatology and Center of Glial Biology in Medicine at the University of Alabama School of Medicine, UAB Women and Infant Center, University of Alabama at Birmingham, 1700 6th Ave South, Birmingham, AL 35294, USA

<sup>2</sup> RNA Biology and Epigenetics Laboratory, Department of Oral and Maxillofacial Surgery, School of Dentistry, University of Alabama at Birmingham, 1919 7th Avenue South, Birmingham, AL 35294, USA

## Introduction

Microglia, the resident immune cells of the central nervous system (CNS), are vital for axonal growth, immune surveillance, and maintenance of the neuronal circuitry. However, under hyperinflammatory conditions, they have deleterious effects on the surrounding brain tissue, thereby contributing to neuroinflammatory diseases. Microglia are the first responders to CNS injury and infiltration by foreign bodies. The activated microglia protect against various brain insults, but they also induce injury by initiating phagocytosis and secreting multiple toxic cytokines, chemokines, and reactive oxygen



© The Author(s) 2025. **Open Access** This article is licensed under a Creative Commons Attribution-NonCommercial-NoDerivatives 4.0 International License, which permits any non-commercial use, sharing, distribution and reproduction in any medium or format, as long as you give appropriate credit to the original author(s) and the source, provide a link to the Creative Commons licence, and indicate if you modified the licensed material. You do not have permission under this licence to share adapted material derived from this article or parts of it. The images or other third party material in this article are included in the article's Creative Commons licence, unless indicated otherwise in a credit line to the material. If material is not included in the article's Creative Commons licence and your intended use is not permitted by statutory regulation or exceeds the permitted use, you will need to obtain permission directly from the copyright holder. To view a copy of this licence, visit <http://creativecommons.org/licenses/by-nc-nd/4.0/>.

intermediates [1, 2]. Hypoxic-ischemic related brain damage in neonates is caused largely by microglial activation, which can be downregulated by inhibiting nuclear factor  $\kappa$  light-chain enhancer of activated B cells (NF- $\kappa$ B) signaling [3]. Neonates, especially preterm infants, are also highly susceptible to infection, which results in a hyperinflammatory response and white matter loss with associated cognitive deficits [4, 5]. The Gram-negative bacteria that often cause these infections induce a dysregulated microglial response compared to the more regulated activation response from other inducers [4]. Microglia in the preterm infant brain respond to both infectious and sterile potentiators of neuroinflammation. Sterile inflammation invokes an immunologic response without initiation by a pathogen. This can be propagated by the systemic release of cytokines from a chronic inflammatory state and by autoimmune diseases such as multiple sclerosis [5–7]. Neuroinflammation causes neurodevelopmental damage that predisposes the infant to learning disorders, autism, schizophrenia, and epilepsy, among other disorders [8–10].

Lipopolysaccharide (LPS) is a potent Gram-negative bacterial endotoxin that drives systemic inflammation in neonates and is an adjuvant for an adaptive immune response [11, 12]. In response to LPS-induced endotoxemia, various types of brain cells synthesize cytokines. Subsequently, peripheral granulocytes invade the CNS through the compromised blood–brain barrier, resulting in immunoreactivity and injury in the affected brain area [1, 2, 13–15]. LPS-induced neuroinflammation can lead to microglial activation associated periventricular WM loss [5]. Microglial activation leads to the signaling of the nuclear factor  $\kappa$  light-chain enhancer of activated B cells (NF- $\kappa$ B) pathway, which causes the release of proinflammatory chemokines and cytokines, such as interleukin (IL)-1 $\beta$ , IL-6, IL-8, IL-18, and tumor necrosis factor- $\alpha$  (TNF- $\alpha$ ). It also facilitates the production of key propagators of inflammation, CD40 and NLRP3. Both of these cause a secondary increase in proinflammatory cytokine production once their expression is enhanced [16]. Resting microglia show low expression of markers of antigen presentation, including CD40 [17], but after activation, microglia undergo various morphological modifications to express cell surface markers necessary for antigen presentation to T cells [18]. NLRP3 is upregulated by pathogen-associated molecular patterns (PAMPs), such as LPS, and then, through secondary signaling, forms the NLRP3 inflammasome, which activates and secretes proinflammatory cytokines IL-1 $\beta$  and IL-18 [19]. Inflammasome activation can result from an external secondary PAMP/damage-associated molecular pattern (DAMP) [19] or self-recognizing patterns [20, 21]. Microglial CD40 and NLRP3 signaling is important in

the progression of inflammatory disease, neurodegenerative diseases, autoimmune diseases, and traumatic brain injury [19, 22–25].

Due to the severe consequences of microglia-mediated neuroinflammation, therapeutic options to attenuate microglial activation have long been under investigation. Options such as minocycline, edaravone, NSAIDs, caffeine, and azithromycin have shown promise, but adverse effects must be considered especially with long-term use [26–30]. MicroRNAs (miRNA) have demonstrated significant immunomodulatory effects in microglia. Mi-146 downregulates the NF- $\kappa$ B signaling cascade [31]; however, a delivery reservoir is needed to optimally deliver them to microglia. Exosomes derived from human breast milk are a natural carrier of this miRNA and many others [32].

Exosomes are 30–200 nm extracellular vesicles (EVs) derived from mammalian breast milk, blood, urine, semen, saliva, and cerebrospinal fluid [33, 34] that function in intercellular communication and in immunological and pathophysiological processes [1, 2, 32, 33]. They reflect the composition and physiology of their cellular origin, including the proteins, lipids, and nucleic acids they carry [35]. A recent study identified hundreds of miRNA and proteins within human breast milk-derived exosomes (HBME) associated with immunological signaling and diseases. Furthermore, they found three key proteins carried by HBME to have a direct antimicrobial effect [36]. Tetraspanins (CD9, CD63, CD81) are found in abundance on the exosome surface and are used to characterize them. They also may be the mechanism by which exosomes target and access cells as we demonstrated in a past study [37]. CD9 can disrupt the TLR4 complex, thus inhibiting LPS-induced NF- $\kappa$ B signaling [38]. We have also previously shown their capability to protect intestinal epithelial cells from oxidative stress [39]. Another study has shown their ability to protect the intestinal epithelial lining in a necrotizing enterocolitis (NEC) mouse model [40]. Exosomes derived from the blood of young rats can decrease the stroke burden in aged rats by downregulating complement cascade-mediated microglia phagocytosis through the inhibitory capacity of the CD46 protein they carry [41]. Our preliminary data shows that HBME also carry CD46, which has not previously been shown in the literature (Supplement 1). Packaging of cargo is a regulated and specific process [42], so they are expected to consistently generate similar results between batches. The low immunogenicity of HBME is an advantage in the immature and sensitive immune system of preterm infants [43]. Their lipid bilayer allows them to survive transport across the blood–brain barrier and into the parenchyma and spinal cord [44, 45]. Their integrity, separation, and functionality are well preserved after

isolation and storage at  $-80\text{ }^{\circ}\text{C}$  for several months [46], making them a viable option for therapeutic and diagnostic applications.

We propose, for the first time in the literature, that HBME attenuate microglial activation, thus serving as a potential treatment for neuroinflammation in neonates, especially preterm infants. Most infants have access to breast milk and thus to HBME as well. This biologically safe and readily available therapy has the potential to change the entire landscape of neonatal neuroinflammatory conditions and the sequelae of morbidities and mortalities that result. By treating both mouse (BV2) and human (HMC3) LPS-induced microglia to HBME, we demonstrate the novel therapeutic impact of HBME

through molecular and morphological analysis. We hypothesize that HBME attenuate LPS-induced TLR4/NF- $\kappa$ B signaling in mouse and human microglia, thus creating a clear path toward providing HBME as preventive and responsive therapy for the highly vulnerable neonatal population (Fig. 1).

## Materials and methods

### Human breast milk collection

Human breast milk (HBM) was collected at the University of Alabama at Birmingham (UAB) Regional Intensive Care Unit. Breastmilk collection was approved by the UAB Institutional Review Board Protocol N160203002. Samples were recovered from patient feedings that were

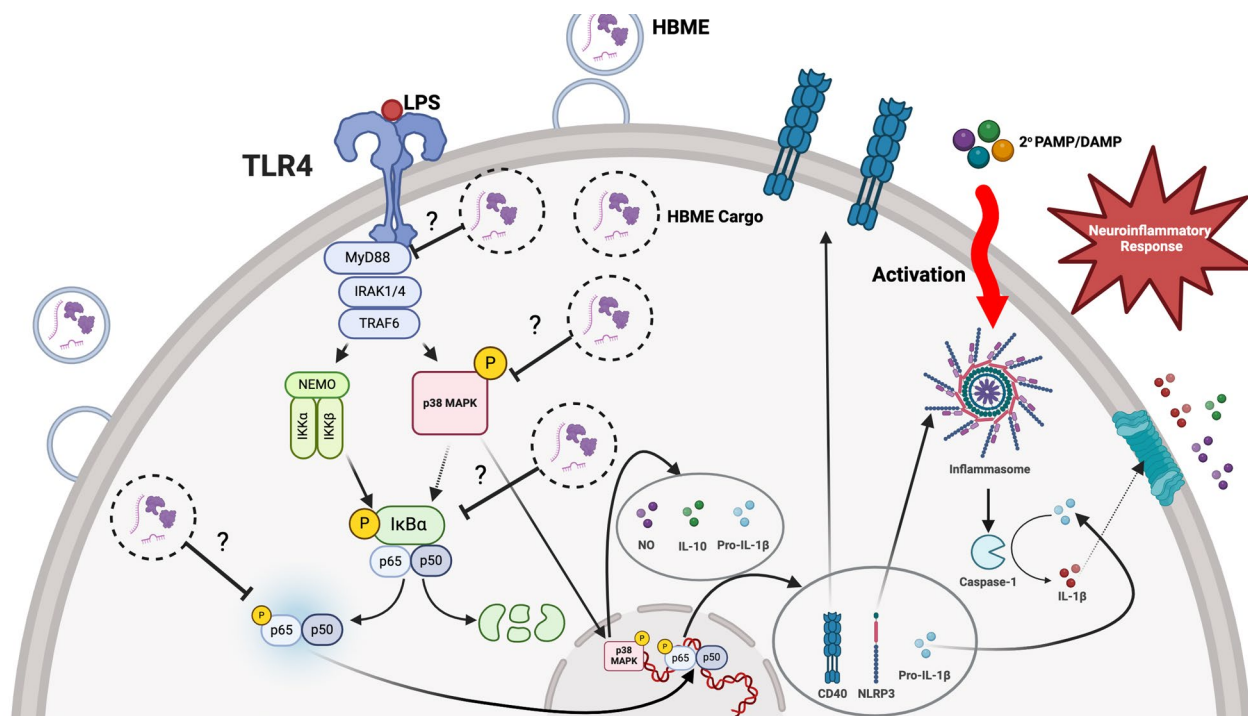


**Fig. 1** HBME inhibit LPS activated canonical NF- $\kappa$ B pathway in microglia and its effectors. HBME seems to enact inhibitory effect either upstream of the TLR4 signaling pathway or directly on different molecules within the cascade. LPS activates the TLR4 receptor causing the activation of two proinflammatory transcription factors, p38 MAPK and the NF- $\kappa$ B p50/p65 heterodimer, ultimately leading to the increased production of key promoters of the microglial immune response. TLR4 relies on the subsequent activation of its adapter protein, MyD88 to potentiate downstream protein activation. The phosphorylated p38 MAPK translocates directly to the nucleus to produce the proinflammatory mediators IL-1 $\beta$  and NO, and the anti-inflammatory cytokine IL-10 through downstream mechanisms. Separately, p38 MAPK further potentiates the activation of NF- $\kappa$ B. The literature suggests that p38 phosphorylates I $\kappa$ B $\alpha$  just as the IKK trimer complex does, thus freeing NF- $\kappa$ B to phosphorylate and translocate to the nucleus where it produces key proinflammatory mediators. CD40 will be incorporated into the plasma membrane to recognize its ligand and further activate microglia. Pro-IL-1 $\beta$  must be cleaved into its active form via the caspase-1 protease found within the NLRP3 inflammasome's multi-protein structure. For NLRP3 to become active and integrated into its inflammasome, a secondary PAMP or DAMP such as the HMGB1 protein must activate it. IL-1 $\beta$  and NO, along with several other proinflammatory cytokines and chemokines, are released from microglia propagating a neuroinflammatory response. Due to these mounting effects, microglial activation can lead to an exaggerated inflammatory response and subsequent CNS toxicity. HBME: Human breast milk derived exosomes; LPS: Lipopolysaccharide; TLR4: Toll-Like Receptor 4; MAPK: Mitogen-activated protein kinases; NF- $\kappa$ B: Nuclear factor kappa B; MyD88: Myeloid differentiation primary response 88; IL-1 $\beta$ : interleukin one beta; NO: nitric oxide; IL-10: interleukin 10; I $\kappa$ B $\alpha$ : Nuclear factor of kappa light polypeptide gene enhancer in B-cells inhibitor alpha; IKK: Inhibitor of nuclear factor- $\kappa$ B kinase; CD40: Cluster of differentiation 40; NLRP3: nucleotide-binding oligomerization domain-like receptor protein 3; PAMP: Pathogen-associated molecular patterns; DAMP: Damage-associated molecular patterns; HMGB1: High mobility group box 1

not completely consumed and would have been discarded. The initial experiments used individual samples; however, to improve consistency, we later pooled donor milk, which was pasteurized using the Holder technique [47]. Milk donors pass a standard health screening to become eligible. Since the milk samples were scavenged, there was no need for ethical consideration. Exosomes in the milk samples were isolated and purified for immediate use or stored at  $-80^{\circ}\text{C}$ .

#### Extracellular vesicle isolation and purification

HBM was diluted 1:10 in sterile phosphate-buffered saline (PBS), centrifuged at  $300\times g$  (1300 revolutions per minute [rpm]) for 10 min, and the supernatant was centrifuged again at  $2600\times g$  (3900 rpm) for another 10 min. The supernatant was filtered through a sterile  $0.22\ \mu\text{m}$  filter using a 10 mL syringe and centrifuged at  $20,000\times g$  (10,800 rpm) for 45 min in an SW41T1 swinging bucket rotor at  $4^{\circ}\text{C}$  using a Beckman Coulter Optima™ L-70 K Ultracentrifuge. The resulting supernatant was further centrifuged at  $110,000\times g$  (32,000 rpm) for 70 min at  $4^{\circ}\text{C}$  using a Beckman Coulter Optima™ L-70 K Ultracentrifuge to collect the EV particles in the pellet, which were resuspended in sterile PBS.

#### Nanoparticle tracking analysis

HBME particle size and concentration were determined by nanoparticle tracking analysis (NTA). The samples were diluted in PBS in a 1 mL disposable syringe. The samples were analyzed using the Nano-Sight NS 300 Sub-Micron Particle Imaging System (Malvern Instruments, Inc., Malvern, UK) and NTA v3.0 software. In this system, a laser light source illuminated the exosome particles, which were then analyzed based on Brownian motion by a semiconductor camera. For each reading frame, the mean values were recorded and analyzed.

#### Transmission electron microscopy

Transmission electron microscopy (TEM) was used to confirm the size and structure of EVs in the exosome samples. Carbon film-coated mesh copper EM-grids were glow discharged at 50 mA for 20 s before loading  $7\ \mu\text{L}$  of the exosome suspension on the grid and incubating for 1 min at room temperature (RT). Samples were stained immediately with  $7\ \mu\text{L}$  of filtered uranyl acetate (UA) solution on the surface of the EM-grid. After 15 s, the excess UA solution was removed, and samples were observed within 24 h under the TEM Tecnai 120 kV (FEI, Hillsboro, OR) at 80 kV and compared to the negatively stained grids. Digital images were captured with a BioSprint 29 CCD camera (AMT, Woburn, MA).

#### Fluorescence-activated cell sorting

For ImageStream analysis, isolated HBME (approximately  $10^7$ – $10^9$  exosome count) were suspended/washed in PBS. The exosomes were fixed with 2% paraformaldehyde for 15 min on ice. Next, they were blocked with anti-human CD16/CD32 APC block for 30 min. They were stained with APC-CD81 (1:100), FITC-CD63 (1:100), and PE-CD9 (1:100) antibodies with the respective isotype controls in  $100\ \mu\text{L}$  of fluorescence-activated cell sorting (FACS) buffer for 30 min and analyzed by ImageStream (BioLegend CA, USA).

#### Microglia cell culture and treatment with LPS and/or HBME

BV2 microglial cells were grown in Roswell Park Memorial Institute (RPMI) 1640 media, supplemented with 10% FBS, 1% penicillin/streptomycin, and  $0.5\ \mu\text{g}/\text{mL}$  amphotericin B (Gibco, Thermo Fisher Scientific, Rockford, IL, USA). Human cell line 3 (HMC3) microglial cells (ATCC, USA) were grown in Eagle's Minimum Essential Media (EMEM), supplemented with 11.2% fetal bovine serum, 1% penicillin/streptomycin, and  $0.5\ \mu\text{g}/\text{mL}$  amphotericin B (Gibco, Thermo Fisher Scientific, Rockford, IL, USA). Glial cells at 70–80% confluency were transferred to 6-well plates and treated with the four following conditions: (1) PBS (normal control), (2) 100 ng/mL or  $1\ \mu\text{g}/\text{mL}$  of LPS, (3) 5 or  $10\ \mu\text{g}/\text{mL}$  of HBME, or (4) simultaneously with LPS (100 ng or  $1\ \mu\text{g}/\text{mL}$ ) and HBME (5 or  $10\ \mu\text{g}/\text{mL}$ ) simultaneously for 0, 0.25, 0.5, 1, or 24 h.

#### Cell viability

Cell viability was measured by trypan blue staining in the Invitrogen Countess 2 automated cell counter. In brief,  $10\ \mu\text{L}$  of 0.4% trypan blue solution was mixed with  $10\ \mu\text{L}$  of the sample, and the device was used to measure cell number and viability in  $10\ \mu\text{L}$  of the mixture on a microscope slide.

#### mRNA sequencing (mRNA-seq) analysis

RNA was extracted from microglial cells using  $0.75\ \text{mL}$  Trizol LS reagent (ThermoFisher Scientific, USA) per  $0.25\ \text{mL}$  of BV2 cell pellet. Samples were homogenized, centrifuged at  $12,000\times g$  for 5 min at  $4^{\circ}\text{C}$ , and incubated for 2–5 min after adding  $0.2\ \text{mL}$  of chloroform. The aqueous phase was collected after centrifugation at  $12,000\times g$  for 15 min at  $4^{\circ}\text{C}$ . RNA in the pellet was washed in 75% ice-cold ethanol diluted in DEPC water for 5 min at  $7500\times g$  at  $4^{\circ}\text{C}$  and quantified by Nanodrop. RNA samples from treatment and control groups were tested for quality and processed for mRNA-seq, bioinformatics, and pathway analysis by Novogene NC, USA (<https://en.novogene.com>). Briefly,  $1\ \mu\text{g}$  of RNA was used to generate sequencing libraries on the Illumina HiSeq 2500

platform. A cutadapter software tool was used to remove the adapter sequences. Paired-end clean reads were aligned to the mouse genome (mm10) using the Spliced Transcripts Alignment to a Reference (STAR) software. The mapped reads were generated by FeatureCounts. Differential expression analysis was performed by edgeR (thresholds: fold change > 1.5,  $P < 0.05$ ).

#### RT-qPCR assay

RNA was extracted from BV2 cells using Direct-zol™ RNA MiniPrep (cat#R2052, ZYMO Research) or Trizol method and treated with DNase I and proteinase K to purify the RNA. Then, 500 ng of total RNA was reverse transcribed into cDNA using the PrimeScript™ RT Reagent kit (cat#RR037Q, Takara). Quantitative real-time PCR was performed using Lunar Universal qPCR Master Mix (New England Biolabs, Ipswich, MA, USA). Changes in relative expression were calculated by the  $2^{-\Delta\Delta C_t}$  method, normalized to *GAPDH*. Primer sequences are as follows: *CD40*, F: 5'-TTG TTG ACA GCG GTC CAT CTA-3'; R: 5'-GCC ATC GTG GAG GTA CTG TTT-3'; *GAPDH*, F: 5'-AGG TCG GTG TGA ACG GAT TTG-3'; R: TGT AGA CCA TGT AGT TGA GGT CA-3'.

#### Western blot (WB)

Protein was extracted from cells in Pierce RIPA buffer (Thermo Scientific, USA) with proteinase and phosphatase inhibitors (Millipore Sigma, Burlington, MA, USA). For WB analysis, protein concentrations were estimated using the bichloroacetic acid (BCA) protein assay kit (ThermoFisher Scientific, USA). 10–25 µg of protein from HBME and microglia (BV2 and HMC3) lysates were resolved on 10% sodium dodecyl sulfate–polyacrylamide gel electrophoresis (SDS-PAGE) gels at 100 V. The gels were subsequently electroblotted onto nitrocellulose (ThermoFisher Scientific, Rockford, IL, USA; GVS, Bologna, Italy), polyvinylidene fluoride, or polyvinylidene difluoride (PVDF) (Millipore Sigma, Burlington, MA, USA) membranes at 15 V. Membranes were blocked with 5% non-fat milk (SKU: 30620074-1, BioWorld, Dublin, OH, USA) and detected by overnight incubation with an appropriate dilution of primary antibody (Supplementary Table 1). Membranes were then incubated with an appropriate horseradish peroxidase (HRP)-conjugated secondary antibody (Supplementary Table 1) in 2% non-fat milk (SKU: 30620074-1, BioWorld, Dublin, OH, USA) for 2 h. Membranes were washed with 1× Tris-buffered saline with 0.1% Tween® 20 (TBST) between each incubation step. Protein expression was detected by a chemiluminescent substrate (Cat #: XR92, Alkali Scientific, Fort Lauderdale, FL, USA; Millipore Sigma, Burlington, MA;) followed by exposure of the membrane to film that

was developed in a film processor (SRX 101-A, Konica Minolta Medical and Graphics, INC, Tokyo, Japan).

#### Enzyme-linked immunosorbent assay (ELISA)

Secreted mouse IL-1β (Catalog #: DY401) and IL-10 (Catalog #: DY417) from BV2 microglia and secreted human IL-1β (Catalog #: DY201) from HMC3 microglia were measured in undiluted cell medium supernatants using DuoSet ELISA kits (R&D Systems). Protocol was followed as provided by the company. Absorbance was determined at 450 nm with subtraction of a 570 nm reference wavelength using the Epoch™ microplate reader (BioTek Instruments Inc.).

#### Immunocytochemistry

BV2 and HMC3 cells were treated as previously described except in this case BV2 cells were treated with 5 µg/mL of HBME, while HMC3 were treated with 10 µg/mL. The cells were fixed in 1% PFA and permeabilized with 0.5% Triton X for 15 min each. Cells were blocked in 5% FBS for 30 min. Cells were probed overnight with the appropriate primary antibody: CD40 (1:100, Cell Signaling, Cat #: 86165) or Iba1 (1:100, Thermo Scientific, Catalog # PA5-27436). They were stained in secondary antibody goat anti-rabbit 488 (1:2000, Cell signaling,) for one hour. Cells were then stained with rhodamine phalloidin (100 nM, Cytoskeleton, Cat. # PHDR1) for 30 min before being mounted with ProLong™ Diamond Antifade Mountant with DAPI (Catalog number P36962). The cells were visualized with the Nikon Eclipse 80i scope and imaged using a Photometrics Coolsnap Myo monochrome camera on the Nikon Elements Software.

#### Statistical analysis

The difference between two groups was analyzed using the student's t-test. For multi-group comparisons, one-way ANOVA was used with the Fisher least significant difference test for post-hoc analysis. Due to the relatively low sample size, an outlier and normality test was also performed. Statistical significance was set to  $P < 0.05$ . Analysis was performed with Microsoft Excel and GraphPad Prism. Data are presented as mean ± standard error of the mean (SEM).

## Results

### Characterization of HBME

HBME characterized by NTA and TEM ranged in diameter from 50 to 150 nm (Fig. 2A) [48] moreover, western blot and ImageStream analysis showed exosome markers CD9, CD63, and CD81 on isolated particles (Fig. 2B–D).

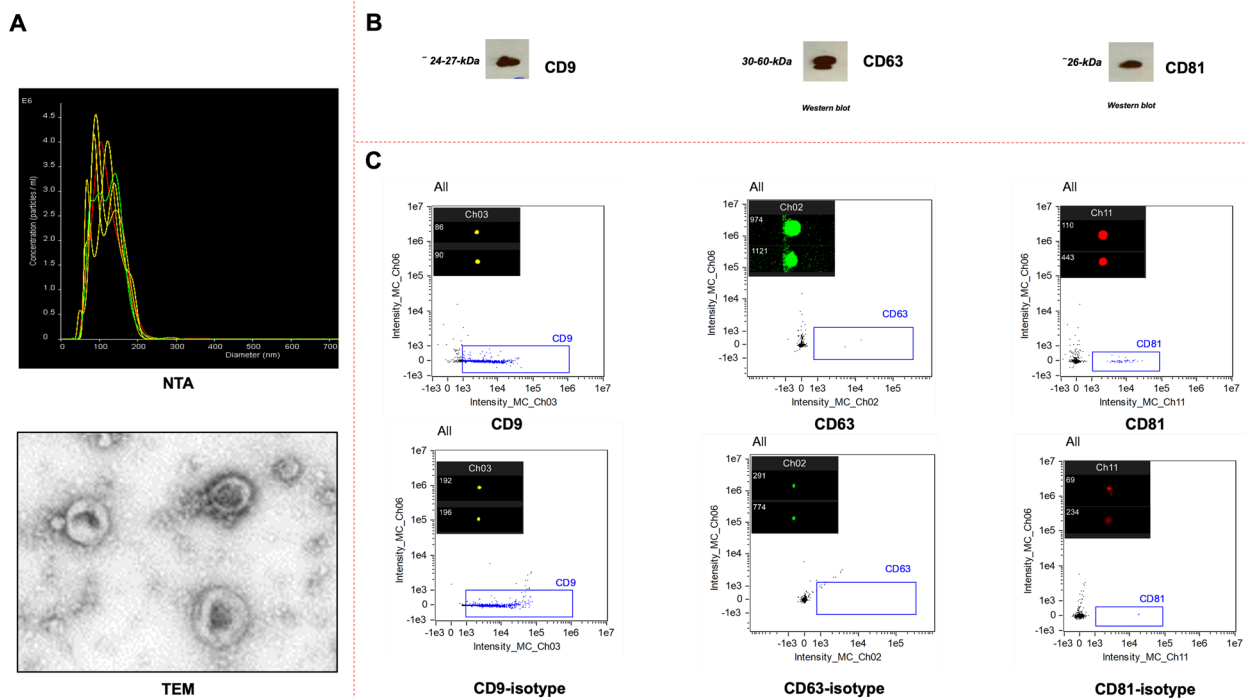


**Fig. 2** Characterization of Human Breast Milk-derived Exosomes. **A** Exosome size, number, and morphology were evaluated using NTA and TEM and were found to be in the expected size range and of the expected morphology. Exosome expression of the tetraspanin molecules CD9, CD63, and CD81 were verified using **B** WB analysis to demonstrate the presence of these exosome-specific markers in exosome protein lysate and **C** FACS analysis to demonstrate their presence on the surface of live, intact exosomes. Each tetraspanin was compared to a IgG isotype control to account for nonspecific binding.  $n \geq 3$ . NTA: Nanosight tracking analysis; TEM: transmission electron microscopy; WB: western blot; FACS: fluorescence-activated cell sorting

### HBME increase the viability of LPS-induced BV2 microglia

BV2 microglia were incubated with LPS (1  $\mu\text{g}/\text{mL}$ ) and HBME (10  $\mu\text{g}/\text{mL}$ ) for 24 h. LPS treatment decreased microglial viability compared to the control ( $P=0.006$ ), which was largely restored by HBME (Fig. 3A;  $P=0.0109$ ). Our data suggest an increase in LPS-induced microglia after HBME treatment. Although there were fewer microglia after LPS induction, there was likely a higher percentage of activated cells, which would account for the increase in proinflammatory markers.

### HBME attenuate CD40 expression in LPS-induced BV2 microglia

The mRNA-seq analysis of BV2 cells incubated with LPS for 24 h identified 156 genes that were downregulated and 17 genes that were upregulated compared to the control (Fig. 3B). The addition of HBME to LPS-stimulated cells led to the downregulation of 136 genes and the upregulation of 25 genes (Fig. 3C). Among the 14 genes that we selected for further analysis, CD40 plays an important role in microglia-mediated hyperinflammatory disease, and its expression in LPS-induced microglia was greatly affected by HBME (Fig. 3D). We confirmed that

HBME downregulated the mRNA (Fig. 3E;  $P=0.0432$ ) and protein expression (Fig. 3F;  $P=0.0093$ ) of the gene encoding CD40 compared to LPS treatment alone by RT-qPCR and WB analysis, respectively.

### HBME modulate intracellular signaling pathway molecules in LPS-induced BV2 and HMC3 microglia

We showed that HBME treatment increases the expression of MyD88 and  $\text{I}\kappa\text{B}\alpha$  while decreasing the activation of p38 MAPK and NF- $\kappa\text{B}$  p65 in BV2 microglia simultaneously stimulated with LPS. MyD88 expression decreased in LPS-induced BV2 microglia compared to the control ( $P=0.037$ ) but increased after treatment with HBME for 1 h compared to the LPS-treated group ( $P=0.0238$ ). Interestingly, after LPS-induced BV2 microglia were treated with HBME, MyD88 expression exceeded the control ( $P=0.0905$ ) and microglia treated with HBME alone ( $P=0.0983$ ) (Fig. 4A).  $\text{I}\kappa\text{B}\alpha$  expression decreased in LPS-induced microglia compared to the control after 1 h ( $P=0.0071$ ) and 24 h ( $P=0.0092$ ) but increased after treatment with HBME for 1 h and 24 h compared to the LPS-treated group (Fig. 4B;  $P=0.0131$  and  $P=0.0063$ , respectively). Treatment of microglial

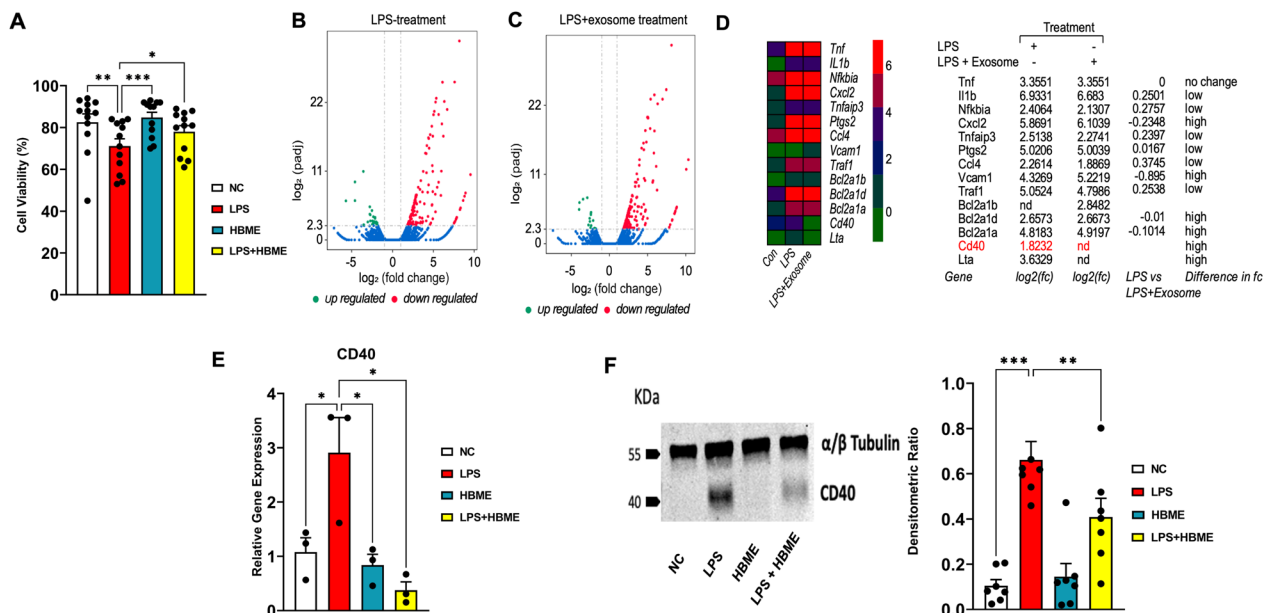


**Fig. 3** Effects of HBME on cell survival and CD40 expression in LPS-induced BV2 microglia. CD40 expression was determined in BV2 microglia treated with PBS (NC), LPS (1 μg/mL), and/or HBME (10 μg/mL) from a single breast milk sample for 24 h. **A** Survival of BV2 microglia cells was measured with trypan blue using a Countess 2 automated cell counter (n = 12). **B, C** Differential expression analysis for LPS-treated or LPS- and HBME-treated microglia. RNA-seq data were analyzed by edgeR (threshold was set as fold change > 1.5, p < 0.05). **D** 14 of the analyzed genes that are important in LPS-induced inflammatory processes were displayed on a heatmap for more direct comparison. **E** RT-qPCR of gene encoding CD40 in multiple experiments (n = 3). **F** WB image for expression of CD40 with densitometry (Image J) analysis for each sample (n = 7). Quantified densitometric ratios normalized to GAPDH. Bars represent the mean ± SEM, n ≥ 3/group, \*p < 0.05, \*\*p < 0.01, \*\*\*p < 0.001, \*\*\*\*p < 0.0001 by ANOVA followed by Fisher’s least significant difference post-hoc multiple comparison test. HBME, human breast milk-derived exosomes

cells with HBME decreased the LPS-induced phosphorylation of p38 MAPK after 15 min (Fig. 4C; P=0.0393) and NF-κB p65 after 1 h (Fig. 4D; P=0.0084). The limitations to using BV2 mouse microglia require demonstration of our findings in other mammalian cells, especially human cells. Thus, we used HMC3 cells to investigate whether HBME attenuate LPS-induced activation in higher-order cell types. We found that HBME down-regulated NF-κB p65 activation in LPS-induced HMC3 microglia (Fig. 7A; P=0.0081).

**HBME decrease the expression of intracellular inflammatory markers and morphological changes in LPS-induced BV2 and HMC3 microglia**

The decrease in the activation of transcription factors NF-κB p50/p65 and p38 MAPK after treatment of LPS-induced BV2 microglia with HBME also affected expression of the CD40, NLRP3, IL-1β, and IL-10 effector molecules. Expression of CD40, NLRP3, and IL-1β increased after LPS treatment but decreased after the addition of HBME (Fig. 5A–C; P=0.026, P=0.0365, and P=0.031). In contrast, expression of IL-10 in LPS-induced BV2 microglia decreased compared to the control (P<0.0001) and increased after treatment with HBME (Fig. 5D; P=0.0177). Additionally, the expression

of CD40 on imaging of LPS-induced BV2 microglia had a demonstrative decrease in expression with HBME costimulation. A similar effect on Iba-1 expression was noted in LPS-induced HMC3 microglia. Both LPS-induced cell types showed a return to morphology more representative of resting microglia after HBME costimulation (Fig. 6).

**HBME alter the secretion of cytokines from LPS-induced BV2 and HMC3 microglia**

Using ELISA, we demonstrated that treatment of microglial cells with HBME reduced LPS-mediated IL-1β secretion in BV2 and HMC3 cells (Fig. 5E, P=0.0301; Fig. 7B, P=0.2709, respectively). HBME also increased IL-10 secretion from LPS-induced BV2 microglia (Fig. 5F; P=0.0178). These results demonstrate the anti-inflammatory effects of HBME. Further experiments are needed to confirm cytokine response in HMC3 microglia.

**Discussion**

Our results indicate that HBME inhibit the expression of LPS-induced proinflammatory proteins in microglia. As preterm neonates are very vulnerable, we need biologically safe and readily available therapeutics to

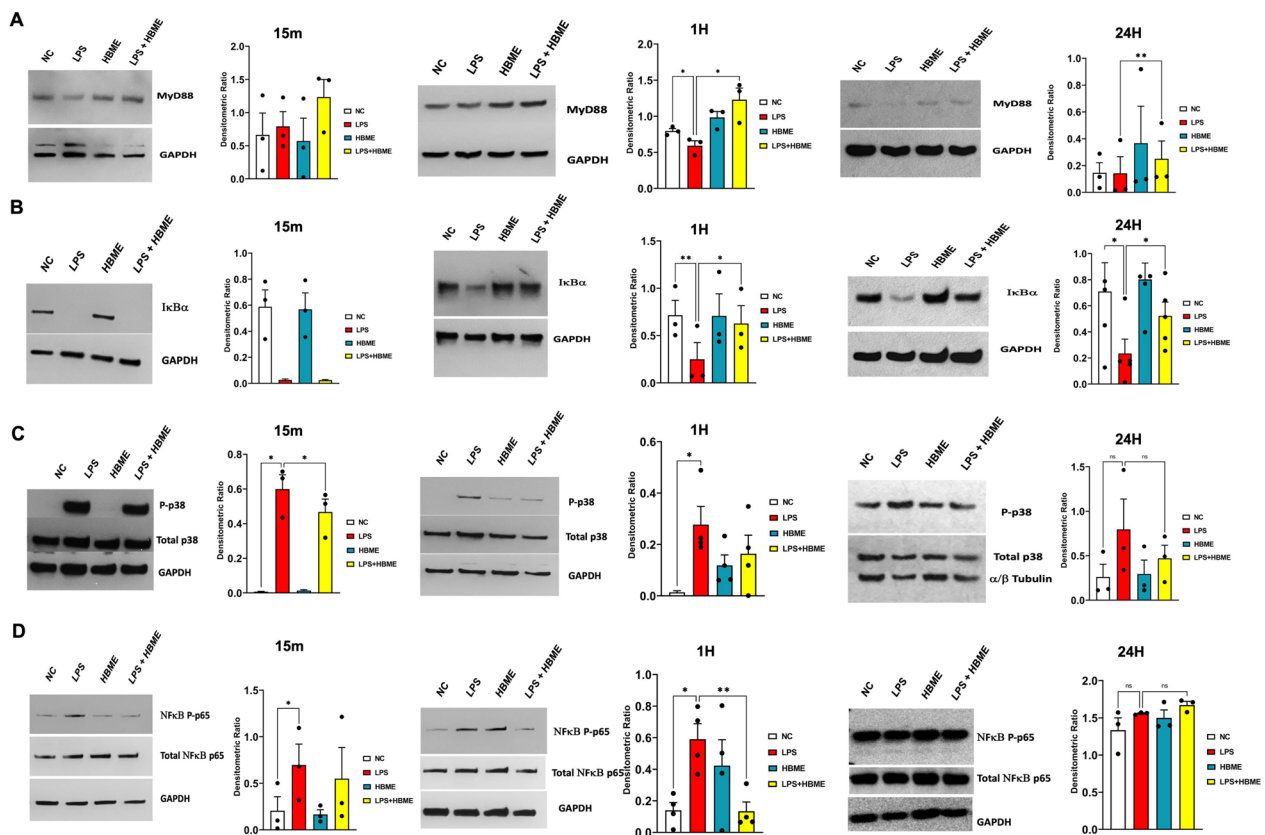


**Fig. 4** Effects of HBME on the TLR4/NF-κB signaling pathways in LPS-induced BV2 microglia. Expression of proteins in the NF-κB pathway affected by LPS stimulation of microglia was determined by WB analysis. Cells were treated with PBS (NC), LPS (1 μg/mL), and/or HBME (10 μg/mL) for 15 min, 1 h, or 24 h. Quantified densitometric ratios normalized to GAPDH (A, B) or total p38 (C)/total NFκB p65 (D). Representative WB images of A MyD88, B IκBa, C MAP kinase p38, and D NF-κB p65 after exposure to experimental conditions are disclosed. Densitometry (Image J) analysis for each sample. Bars represent mean ± SEM, n = 3, \*p < 0.05, \*\*p < 0.01, \*\*\*p < 0.001, \*\*\*\*p < 0.0001 by one-way ANOVA followed by Fisher's least significant difference post-hoc multiple comparison test

combat common neonatal pathologies. Human breast milk exosomes can protect against NEC [49, 50] and microbial infections [36]. These exosomes contain cargo that has significant anti-inflammatory potential. Bovine milk exosomes carry signaling proteins for immune cell receptors, phagocytosis, and cytotoxicity [51], and HBME are likely to have the same properties. As intestinal diseases such as NEC often lead to neurodevelopmental delays in preterm neonates and has been extensively studied [52, 53], we aimed to add perspective on the much needed area of neuroprotective potential of exosomes. Systemic illness originating from various sources leads to brain injury largely resulting from microglial activation [54–56]. We targeted microglia as both exosomes and microglia regulate the immune response and inflammation.

Among the many genes showing LPS-induced changes in expression, the gene encoding CD40 was the most interesting because upregulation of the CD40 receptor amplifies the immune cell response in human microglia

[57], exaggerating the neuroinflammatory response and potentially increasing autoinflammatory disease [58, 59]. The role of microglia in CNS disorders such as multiple sclerosis and Alzheimer's disease [60, 61] prompted our interest in the regulation of CD40 expression in these cells. The expression of the CD40 receptor on the surface of microglia orchestrates peripheral leukocyte infiltration and retention in the CNS [62]. Compared to the adult brain, the neonatal immune system is immature, but it mounts a robust response, especially to the LPS endotoxin [8–10, 43]; thus, CD40 may play a key role in this process. Our results on the effects of HBME on BV2 microglial cell survival and CD40 expression (Fig. 3) led us to investigate the intracellular pathway(s) affected by HBME that underlie this change in CD40 expression. The morphological changes and proinflammatory mediator response inhibited by HBME in BV2 and HMC3 cells also led us to investigate internal mechanisms (Fig. 6).

LPS induces the binding of transcription factor NF-κB p50/p65 to the promoter of the gene encoding CD40 in

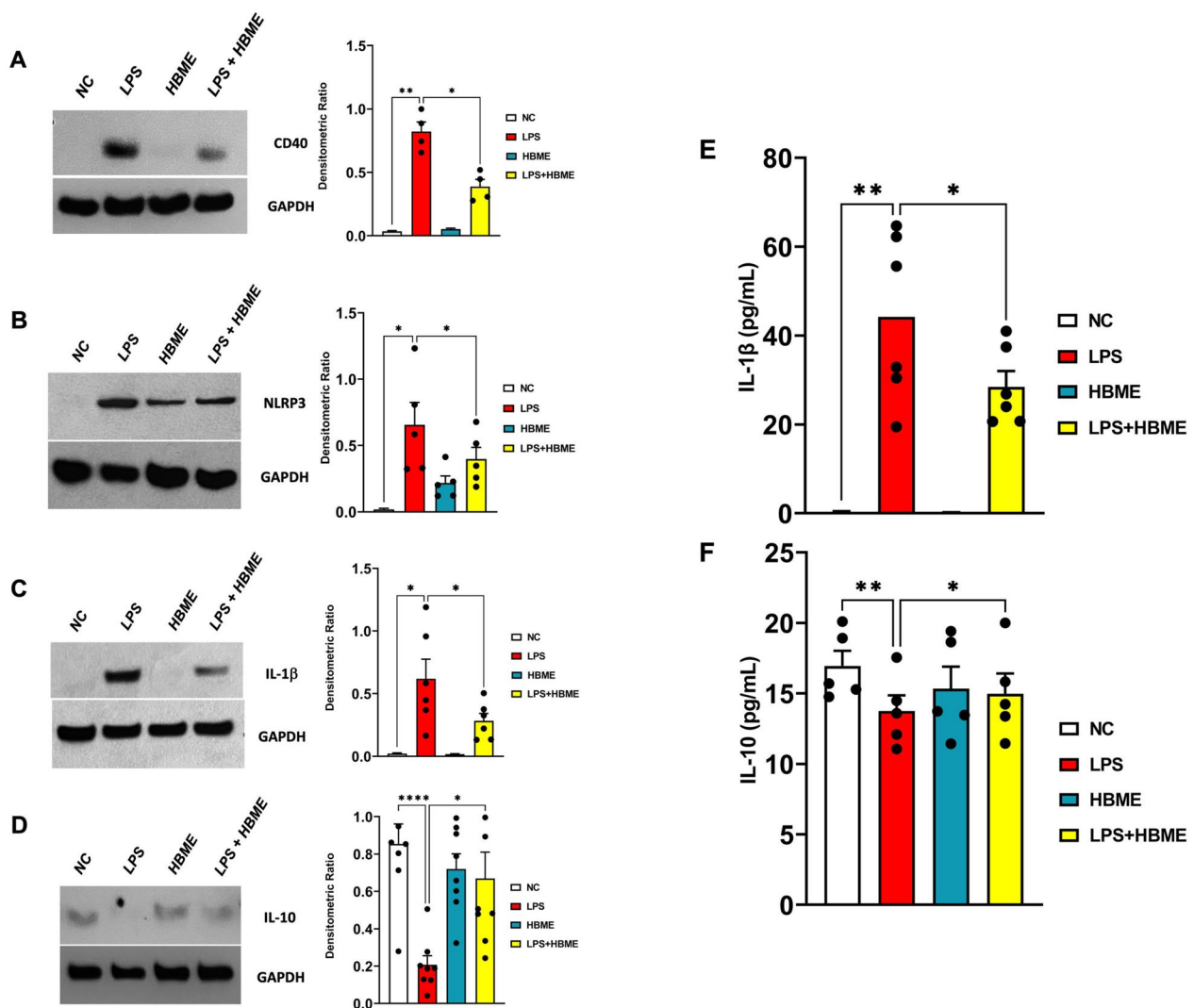


**Fig. 5** Effects of HBME on inflammatory markers in LPS-induced BV2 microglia. Expression of NF-κB pathway downstream effectors of inflammation by LPS stimulation of microglia was determined by WB analysis and ELISA. Cells were treated as previously described for 24 h. Quantified densitometric values were graphed and representative WB images were disclosed for **A** CD40 (n=4), **B** NLRP3 (n=5), **C** IL-1β (n=6), and **D** IL-10 (n=8). Densitometric (Image J) analysis for each sample. ELISA analysis represented for **E** IL-1β (n=6) and **F** IL-10 (n=5). Bars represent mean ± SEM, n ≥ 3, \*p < 0.05, \*\*p < 0.01, \*\*\*p < 0.001, \*\*\*\*p < 0.0001 by one-way ANOVA followed by Fisher’s least significant difference post-hoc multiple comparison test

microglial nuclei via the TLR4 pathway [17, 63, 64]. We demonstrated that HBME inhibited the activation of the p65 component in the p50/p65 heterodimer by decreasing the expression and activation of MyD88, IκBα, and p38 MAPK, which are key molecules upstream of the TLR4 pathway [65–67]. Without activation of MyD88, TLR4 will not activate, and the IKK complex and p38 MAPK will also fail to activate, thereby arresting the NF-κB pathway [20, 21]. Our results show a decrease in MyD88 expression in LPS-induced BV2 microglia, in contrast to the increase seen in previous studies [66, 68, 69]. HBME not only restored the protein level but also

increased expression above the control. The difference in MyD88 expression in our study may be due to the shorter time of exposure compared to previous studies [69]. The differences may also reflect negative feedback through ubiquitination or deubiquitination of MyD88, leading to receptor internalization/downregulation and/or proteasomal degradation after LPS treatment [70–72]. Furthermore, the ability of HBME to upregulate MyD88 (Fig. 4A) may be due to the capacity of some proteins carried by exosomes to alter the signaling of immune cell receptors [51]. How this leads to the downregulation of downstream molecules requires further investigation.

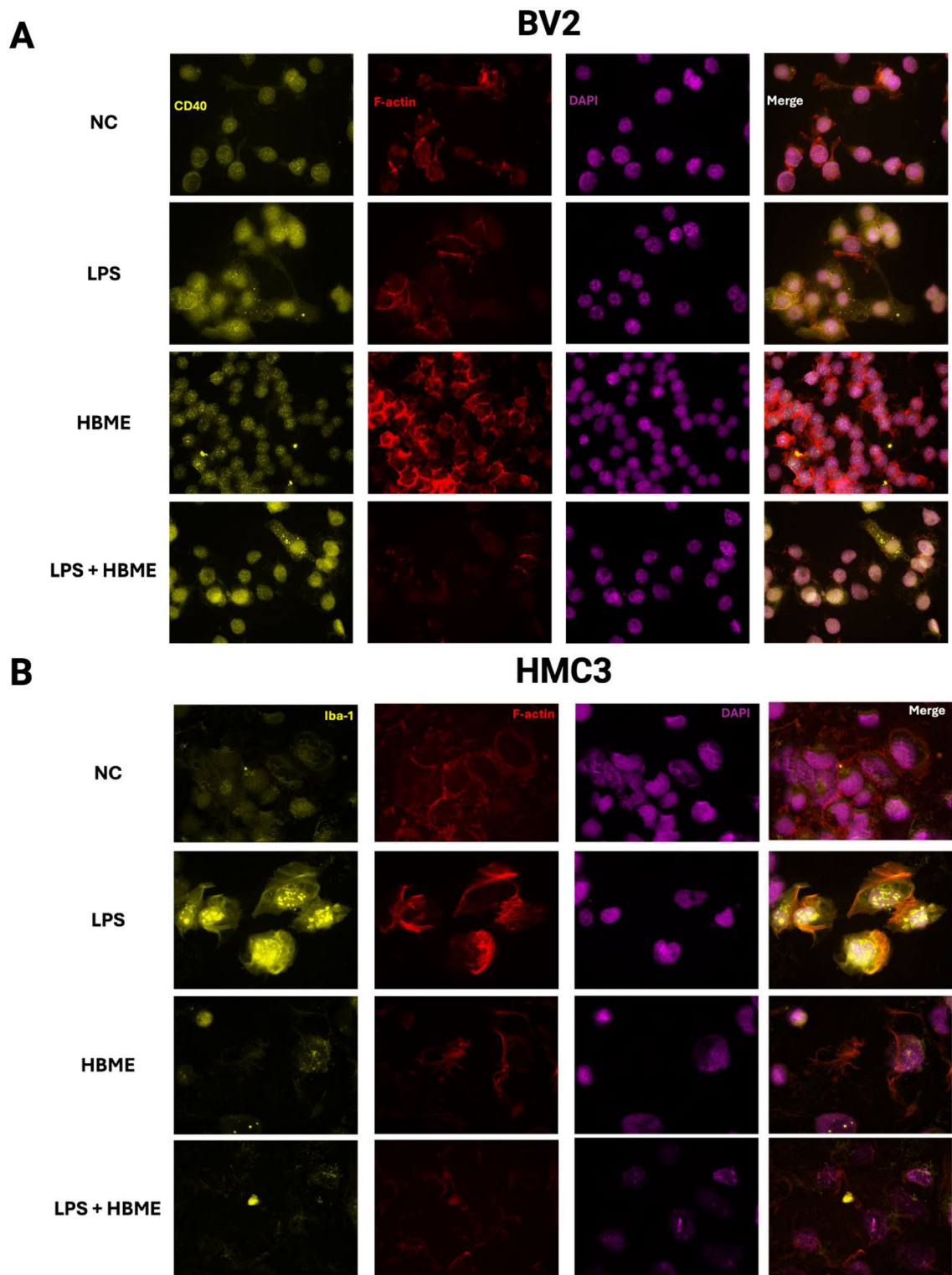


**Fig. 6** HBME inhibit the proinflammatory response and morphological changes of LPS-induced microglia. Immunofluorescence staining on microglial cells demonstrates HBME-mediated reduction in morphological changes and proinflammatory marker expression reflective of LPS-induced microglial activation. **A** BV2 microglia were treated with PBS (NC), LPS (1  $\mu\text{g}/\text{mL}$ ), and/or HBME (5  $\mu\text{g}/\text{mL}$ ) for 24 h and probed for CD40, phalloidin (F-actin), and DAPI. **B** HMC3 microglia were treated with PBS (NC), LPS (1  $\mu\text{g}/\text{mL}$ ), and/or HBME (10  $\mu\text{g}/\text{mL}$ ) for 4 h and probed for Iba-1, phalloidin (F-actin), and DAPI

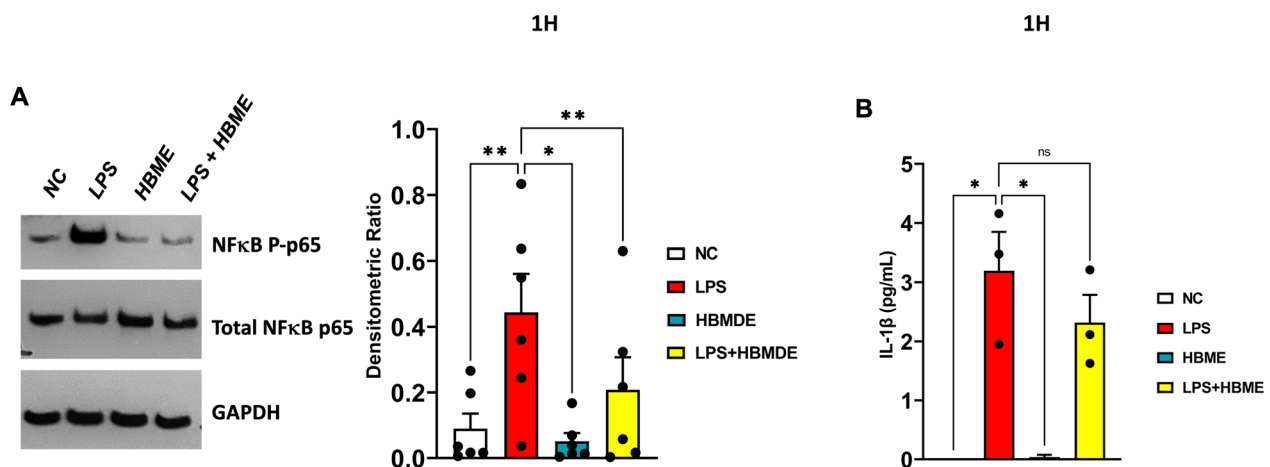


**Fig. 7** Effects of HBME on intracellular signaling and cytokine secretion from LPS-induced HMC3 microglia. Expression of proteins in the NF- $\kappa$ B pathway affected by LPS and/or HBME stimulation of microglia was determined by WB and ELISA analysis. Cells were treated with PBS (NC), LPS (1  $\mu$ g/mL), and/or HBME (10  $\mu$ g/mL) for 1 h. **A** Representative WB image and the quantified densitometric ratios normalized to GAPDH of NF $\kappa$ B p65 are shown (n=6). **B** ELISA analysis of IL-1 $\beta$  secretion from cells into the media represented (n=3). Bars represent mean  $\pm$  SEM, n  $\geq$  3, \*p < 0.05, \*\*p < 0.01, \*\*\*p < 0.001, \*\*\*\*p < 0.0001 by one-way ANOVA followed by Fisher's least significant difference post-hoc multiple comparison test

I $\kappa$ B $\alpha$  is targeted for proteasomal degradation [73]. Our data indicated that HBME directly and indirectly stabilized I $\kappa$ B $\alpha$  in the BV2 cytoplasm, thereby increasing its adherence to p50/p65 compared to the untreated LPS group (Fig. 4B) [65, 67]. Decreased p38 MAPK expression after HBME treatment in BV2 microglia (Fig. 4C) will decrease activation of its downstream kinases, MK2 and MSK1/2, thereby decreasing NF- $\kappa$ B p50/65 functionality and proinflammatory cytokine production. MSK1/2 independently promotes the expression of anti-inflammatory cytokines IL-10 and the IL-1 receptor antagonist (IL-1ra) and promotes the dephosphorylation of p38 through a negative feedback loop after its initial proinflammatory effects [74]. MSK1/2 is inhibited by MK2 [75], which may account for the increase in intracellular and secreted IL-10 (Figs. 5D and 6B). Activation of I $\kappa$ B $\alpha$  by p38 MAPK will also be mitigated when MK2 inhibits MSK1/2 [65, 67]. HBME may initiate a switch in MSK1/2 and inhibit p38 MAPK directly to promote its anti-inflammatory effects in microglia more quickly. These changes caused by HBME culminate in the decreased phosphorylation of NF- $\kappa$ B p65 (Figs. 4D and 7A), and the activation of the p65 component is largely responsible for the transcriptional activity of the p50/p65 heterodimer [76].

Neuroinflammation is mediated by the secretion of proinflammatory cytokines, especially the potent IL-1 $\beta$  [77], from various cells in the brain, particularly microglia and invading immune cells. HBME treatment of BV2 and HMC3 microglia decreased the production and secretion of IL-1 $\beta$  (Figs. 5C, 6A and 7B), inducing microglial hyperactivation because IL-1 $\beta$  stimulates microglial

signaling through its receptor along with LPS-TLR4 signaling [77]. IL-1 $\beta$  must be activated to cause cellular changes, and the NLRP3 inflammasome activates IL-1 $\beta$ . The decrease in NLRP3 and IL-1 $\beta$  expression observed in microglia (Fig. 5B, C) suggests that NLRP3 inflammasome activation also decreased.

IL-10 counters proinflammatory effector molecules [78, 79] thus, a deficiency in this anti-inflammatory cytokine is linked to chronic inflammatory conditions, such as inflammatory bowel diseases, enteropathies, and autoimmune disorders, and to exacerbation of chronic organ conditions such as liver and kidney disease, and hypersensitive disorders, such as asthma [4]. Recombinant IL-10 was used to treat autoimmune and chronic inflammatory diseases in mouse and human trials, respectively [80, 81]. T cells are an abundant source of IL-10, and their response is decreased by IL-10 [4, 82]. IL-10 may also decrease CD40L presentation to LPS-induced microglia that are highly expressing CD40 because T cells commonly express CD40L [83]. Although most immune cells secrete IL-10 during inflammation, a delayed response results in significant brain insult before IL-10 can counter those effects [84]. Here, we demonstrated that HBME induced the production and secretion of IL-10 by microglia (Fig. 5D; Fig. 6B). Co-culture studies with microglia and T cells would provide further insight into the role of IL-10 in HBME-mediated anti-inflammatory effects.

The temporal sequence of gene expression and enzyme activation is critical in transcriptional programs, but the transcription of genes is often transient. For example, LPS-induced activation of NF- $\kappa$ B p50/p65 via MyD88-dependent pathways leads to its association with the

CD40 promoter, while p38 MAPK's activation promotes MK2 to become associated with the IL-1 $\beta$  promoter region [65, 67, 85–88]. Thus, the expression and activity of pathway molecules were affected within one hour of LPS induction and HBME treatment. The response of I $\kappa$ B $\alpha$  to LPS and HBME treatment at both one h and 24 h suggests either a wide timeframe for expression of this molecule or a biphasic response due possibly to its role in different pathways, such as tumor suppressor p53 [89]. This may also be a species-specific response, as this was observed solely in BV2 cells. Thus, it is critical to identify a rapid response for the treatment of neonates. This study is limited by the genotypic/phenotypic differences common in *in vitro* studies and immortalized cell lines. The confirmation of these findings in human microglia showing the ability of HBME to downregulate NF- $\kappa$ B p65 and IL-1 $\beta$  in the microglia-mediated inflammatory cascade implies that this treatment may be translational to human subjects. Here, HBME is a suppressor of LPS-induced signaling and proinflammatory output in HMC3 microglia. These results must be confirmed in animal studies, and further studies are needed to develop HBME as a novel and safe therapy for preterm neonates.

## Conclusion

We demonstrated that HBME decreased the production of proinflammatory mediators CD40, NLRP3, and IL-1B by inhibiting the TLR4/MyD88/NF- $\kappa$ B signaling pathway in LPS-induced BV2 microglia. The findings in HMC3 microglia imply that HBME affect human microglia in similar manner to that shown in mouse microglia. Treatment of neonates requires a rapid response to an infectious or sterile insult; thus, this study provides evidence to further study the role of HBME as a strategic intervention in neuroinflammation.

## Abbreviations

CNS	Central nervous system
LPS	Lipopolysaccharide
NEC	Necrotizing enterocolitis
TLR4	Toll-like receptor 4
NF- $\kappa$ B	Nuclear factor $\kappa$ light-chain enhancer of activated B cells
IL	Interleukin
TNF- $\alpha$	Tumor necrosis factor-alpha
IKK	Inhibitor of nuclear factor- $\kappa$ B kinase
MAPK	Mitogen-activated protein kinase
I $\kappa$ B $\alpha$	Nuclear factor of kappa light polypeptide gene enhancer in B-cells inhibitor alpha
MK2	Mitogen-activated protein kinase-activated protein kinase 2
MSK	Mitogen- and stress-activated kinase
MyD88	Myeloid differentiation primary response 88
CD	Cluster of differentiation
NLRP3	Nucleotide-binding oligomerization domain-like receptor protein 3
CD40L	CD40 ligand
MIP-1	Macrophage inflammatory protein 1
TRAF	Tumor necrosis factor receptor-associated factor
STAT	Signal transducer and activator of transcription
PAMP	Pathogen-associated molecular pattern

DAMP	Damage-associated molecular pattern
NEK7	NIMA-related kinase 7
ASC	Apoptosis-associated speck-like protein containing CARD
HMGB1	High mobility group box 1
EV	Extracellular vesicle
HBME	Human breast milk-derived exosomes
HBM	Human breast milk
PBS	Phosphate-buffer saline
NTA	Nanoparticle tracking analysis
TEM	Transmission electron microscopy
UA	Uranyl acetate
RPMI	Roswell Park Memorial Institute
HMC3	Human microglia cell line 3
FACS	Fluorescence-activated cell sorting
STAR	Spliced Transcripts Alignment to a Reference
BCA	Bichloroacetic acid
WB	Western blot
HRP	Horseshoe peroxidase
ELISA	Enzyme-linked immunosorbent assay
TNFAIP3	Tumor necrosis factor $\alpha$ -induced protein 3
IFN- $\beta$	Interferon- $\beta$

## Supplementary Information

The online version contains supplementary material available at <https://doi.org/10.1186/s12974-025-03345-2>.

Supplementary Material 1.  
Supplementary Material 2.  
Supplementary Material 2.

## Acknowledgements

We thank the University of Alabama's high-resolution imaging service center for assistance with NTA and TEM. We thank Jarren Oates, PhD for his invaluable contributions to the execution of the experiments.

## Author contributions

OTA, SK, BS, and QH contributed to the experimental design and writing the manuscript. OTA, SK, YC, and BT executed the experiments and provided input. OTA, SK, YC, QH and BS prepared figures. All authors were able to review the manuscript before submission.

## Funding

This work was supported by the National Institutes of Health (1R15DA045564-01) and #5R25MH080661-13/2004445114.

## Availability of data and materials

The supporting data for this study are available from the corresponding author upon reasonable request. Data in supplemental data section.

## Declarations

### Ethics approval and consent to participate

Ethics approval and consent to participate were not needed. BV2 cells were a generous gift from Dr. Harald Neumann at the University of Bonn LIFE and Brain Center in Bonn, Germany.

### Consent for publication

Not applicable.

### Competing interests

The authors declare no competing interests.

Received: 29 July 2024 Accepted: 13 January 2025

Published online: 15 February 2025

## References

- Zhou Q, Guo D, Li X, Wang Y, Ye X, Xue S, et al. Anti-inflammatory effects of vinpocetine in LPS-stimulated microglia via activation of AMPK. *Acad Bras Ciênc*. 2020;92(4): e20200241.
- Sousa NA, Oliveira GAL, De Oliveira AP, Lopes ALF, Iles B, Nogueira KM, et al. Novel ocellatin peptides mitigate LPS-induced ROS formation and NF- $\kappa$ B activation in microglia and hippocampal neurons. *Sci Rep*. 2020;10(1):2696.
- Li B, Dasgupta C, Huang L, Meng X, Zhang L. MiRNA-210 induces microglial activation and regulates microglia-mediated neuroinflammation in neonatal hypoxic-ischemic encephalopathy. *Cell Mol Immunol*. 2020;17(9):976–91.
- Shemer A, Scheyltjens I, Frumer GR, Kim J-S, Grozovski J, Ayanaw S, et al. Interleukin-10 prevents pathological microglia hyperactivation following peripheral endotoxin challenge. *Immunity*. 2020;53(5):1033–49.e7.
- Dean JM, van de Looij Y, Sizonenko SV, Lodygensky GA, Lazeyras F, Bolouri H, et al. Delayed cortical impairment following lipopolysaccharide exposure in preterm fetal sheep. *Ann Neurol*. 2011;70(5):846–56.
- Favrais G, van de Looij Y, Fleiss B, Ramanantsoa N, Bonnin P, Stoltenburg-Didinger G, et al. Systemic inflammation disrupts the developmental program of white matter. *Ann Neurol*. 2011;70(4):550–65.
- Plastini MJ, Desu HL, Brambilla R. Dynamic responses of microglia in animal models of multiple sclerosis. *Front Cell Neurosci*. 2020;14:269.
- Zhan Y, Paolicelli RC, Sforzini F, Weinhard L, Bolasco G, Pagani F, et al. Deficient neuron-microglia signaling results in impaired functional brain connectivity and social behavior. *Nat Neurosci*. 2014;17(3):400–6.
- Bright HR, Babata K, Allred EN, Erdei C, Kuban KCK, Joseph RM, et al. Neurocognitive outcomes at 10 years of age in extremely preterm newborns with late-onset bacteremia. *J Pediatr*. 2017;187:43–9.e1.
- Salas AA, Faye-Petersen OM, Sims B, Peralta-Carcelen M, Reilly SD, Mcgwin G, et al. Histological characteristics of the fetal inflammatory response associated with neurodevelopmental impairment and death in extremely preterm infants. *J Pediatr*. 2013;163(3):652–7.e2.
- Ganesh V, Bodewits K, Bartholdson SJ, Natale D, Campopiano DJ, Mareque-Rivas JC. Effective binding and sensing of lipopolysaccharide: combining complementary pattern recognition receptors. *Angew Chem Int Ed Engl*. 2009;48(2):356–60.
- Kim YS, Ryu JH, Han SJ, Choi KH, Nam KB, Jang IH, et al. Gram-negative bacteria-binding protein, a pattern recognition receptor for lipopolysaccharide and beta-1,3-glucan that mediates the signaling for the induction of innate immune genes in *Drosophila melanogaster* cells. *J Biol Chem*. 2000;275(42):32721–7.
- Hang CH, Shi JX, Tian J, Li JS, Wu W, Yin HX. Effect of systemic LPS injection on cortical NF- $\kappa$ B activity and inflammatory response following traumatic brain injury in rats. *Brain Res*. 2004;1026(1):23–32.
- Liu C, Sun SQ, Yu JB, Wang KJ, Xu Q, Chen H, et al. Expression of neuroglobin in rats with brain injury induced by LPS. *Zhonghua Shao Shang Za Zhi*. 2009;25(3):222–6.
- Lyu Y, Fu L, Li Y, Wen J, Wei X, Qian Y. Microvesicles derived from LPS-induced microglia aggravate the injury of tight junction in rat brain microvascular endothelial cells under oxygen-glucose deprivation. *Xi Bao Yu Fen Zi Mian Yi Xue Za Zhi*. 2018;34(3):211–7.
- Nguyen VT, Benveniste EN. Critical role of tumor necrosis factor- $\alpha$  and NF- $\kappa$ B in interferon- $\gamma$ -induced CD40 expression in microglia/macrophages. *J Biol Chem*. 2002;277(16):13796–803.
- Qin H, Wilson CA, Lee SJ, Zhao X, Benveniste EN. LPS induces CD40 gene expression through the activation of NF- $\kappa$ B and STAT-1 $\alpha$  in macrophages and microglia. *Blood*. 2005;106(9):3114–22.
- Toledano Furman N, Gottlieb A, Prabhakara KS, Bedi S, Caplan HW, Rupert KA, et al. High-resolution and differential analysis of rat microglial markers in traumatic brain injury: conventional flow cytometric and bioinformatics analysis. *Sci Rep*. 2020;10(1):11991.
- Ismael S, Nasoohi S, Ishrat T. MCC950, the selective inhibitor of nucleotide oligomerization domain-like receptor protein-3 inflammasome, protects mice against traumatic brain injury. *J Neurotrauma*. 2018;35(11):1294–303.
- Kim S-W, Oh S-A, Seol S-I, Davaanyam D, Lee J-K. Cytosolic HMGB1 mediates LPS-induced autophagy in microglia by interacting with NOD2 and suppresses its proinflammatory function. *Cells*. 2022;11(15):2410.
- Bai H, Zhang Q. Role of N4-acetylcytidine for continuously activating NLRP3 inflammasome by HMGB1 pathway in microglia. *Neural Regen Res*. 2021;16(7):1427–8.
- Jiang R-H, Xu X-Q, Wu C-J, Lu S-S, Zu Q-Q, Zhao L-B, et al. The CD40/CD40L system regulates rat cerebral microvasculature after focal ischemia/reperfusion via the mTOR/S6K signaling pathway. *Neurol Res*. 2018;40(9):717–23.
- Townsend KP, Town T, Mori T, Lue LF, Shytle D, Sanberg PR, et al. CD40 signaling regulates innate and adaptive activation of microglia in response to amyloid  $\beta$ -peptide. *Eur J Immunol*. 2005;35(3):901–10.
- Dempsey C, Rubio Araiz A, Bryson KJ, Finucane O, Larkin C, Mills EL, et al. Inhibiting the NLRP3 inflammasome with MCC950 promotes non-phlogistic clearance of amyloid-beta and cognitive function in APP/PS1 mice. *Brain Behav Immun*. 2017;61:306–16.
- Coll RC, Robertson AAB, Chae JJ, Higgins SC, Muñoz-Planillo R, Inerra MC, et al. A small-molecule inhibitor of the NLRP3 inflammasome for the treatment of inflammatory diseases. *Nat Med*. 2015;21(3):248–55.
- Ramarao S, Pang Y, Carter K, Bhatt A. Azithromycin protects oligodendrocyte progenitor cells against lipopolysaccharide-activated microglia-induced damage. *Dev Neurosci*. 2022;44(1):1–12.
- Yang L, Yu X, Zhang Y, Liu N, Xue X, Fu J. Caffeine treatment started before injury reduces hypoxic-ischemic white-matter damage in neonatal rats by regulating phenotypic microglia polarization. *Pediatr Res*. 2022;92(6):1543–54.
- Lim GP, Yang F, Chu T, Chen P, Beech W, Teter B, et al. Ibuprofen suppresses plaque pathology and inflammation in a mouse model for Alzheimer's disease. *J Neurosci*. 2000;20(15):5709–14.
- Wang H-M, Zhang T, Huang J-K, Xiang J-Y, Chen J-J, Fu J-L, et al. Edaravone attenuates the proinflammatory response in amyloid- $\beta$ -treated microglia by inhibiting NLRP3 inflammasome-mediated IL-1 $\beta$  secretion. *Cell Physiol Biochem*. 2017;43(3):1113–25.
- Howard R, Zubko O, Bradley R, Harper E, Pank L, O'Brien J, et al. Minocycline at 2 different dosages vs placebo for patients with mild Alzheimer disease. *JAMA Neurol*. 2020;77(2):164.
- Liang C, Zou T, Zhang M, Fan W, Zhang T, Jiang Y, et al. MicroRNA-146a switches microglial phenotypes to resist the pathological processes and cognitive degradation of Alzheimer's disease. *Theranostics*. 2021;11(9):4103–21.
- Zhou Q, Li M, Wang X, Li Q, Wang T, Zhu Q, et al. Immune-related MicroRNAs are abundant in breast milk exosomes. *Int J Biol Sci*. 2012;8(1):118–23.
- Crenshaw BJ, Gu L, Sims B, Matthews QL. Exosome biogenesis and biological function in response to viral infections. *Open Virol J*. 2018;12:134–48.
- Chernyshev VS, Rachamadugu R, Tseng YH, Belnap DM, Jia Y, Branch KJ, et al. Size and shape characterization of hydrated and desiccated exosomes. *Anal Bioanal Chem*. 2015;407(12):3285–301.
- Thakur BK, Zhang H, Becker A, Matei I, Huang Y, Costa-Silva B, et al. Double-stranded DNA in exosomes: a novel biomarker in cancer detection. *Cell Res*. 2014;24(6):766–9.
- Kim KU, Han K, Kim J, Kwon DH, Ji YW, Yi DY, et al. The protective role of exosome-derived microRNAs and proteins from human breast milk against infectious agents. *Metabolites*. 2023;13(5):635.
- Sims B, Farrow AL, Williams SD, Bansal A, Krendelichtchikov A, Matthews QL. Tetraspanin blockage reduces exosome-mediated HIV-1 entry. *Adv Virol*. 2018;163(6):1683–9.
- Suzuki M, Tachibana I, Takeda Y, He P, Minami S, Iwasaki T, et al. Tetraspanin CD9 negatively regulates lipopolysaccharide-induced macrophage activation and lung inflammation. *J Immunol*. 2009;182(10):6485–93.
- Martin C, Patel M, Williams S, Arora H, Brawner K, Sims B. Human breast milk-derived exosomes attenuate cell death in intestinal epithelial cells. *Innate Immun*. 2018;24(5):278–84.
- He S, Liu G, Zhu X. Human breast milk-derived exosomes may help maintain intestinal epithelial barrier integrity. *Pediatr Res*. 2021;90(2):366–72.
- Zhang H, Lin S, Mcelroy CL, Wang B, Jin D, Uteshev VV, et al. Circulating pro-inflammatory exosomes worsen stroke outcomes in aging. *Circ Res*. 2021;129(7): e121.
- Stevanato L, Thanabalasundaram L, Vysokov N, Sinden JD. Investigation of content, stoichiometry and transfer of miRNA from human neural stem cell line derived exosomes. *PLoS ONE*. 2016;11(1): e0146353.

43. Zhao J, Kim KD, Yang X, Auh S, Fu Y-X, Tang H. Hyper innate responses in neonates lead to increased morbidity and mortality after infection. *Proc Natl Acad Sci*. 2008;105(21):7528–33.
44. Gao ZS, Zhang CJ, Xia N, Tian H, Li DY, Lin JQ, et al. Berberine-loaded M2 macrophage-derived exosomes for spinal cord injury therapy. *Acta Biomater*. 2021;126:211–23.
45. Qu M, Lin Q, Huang L, Fu Y, Wang L, He S, et al. Dopamine-loaded blood exosomes targeted to brain for better treatment of Parkinson's disease. *J Control Release*. 2018;287:156–66.
46. Munagala R, Aqil F, Jayabalan J, Gupta RC. Bovine milk-derived exosomes for drug delivery. *Cancer Lett*. 2016;371(1):48–61.
47. Capriati T, Goffredo BM, Argentieri M, De Vivo L, Bernaschi P, Cairoli S, et al. A modified holder pasteurization method for donor human milk: preliminary data. *Nutrients*. 2019;11(5):1139.
48. Admyre C, Johansson SM, Qazi KR, Filén J-J, Lahesmaa R, Norman M, et al. Exosomes with immune modulatory features are present in human breast milk. *J Immunol*. 2007;179(3):1969–78.
49. Wang X, Yan X, Zhang L, Cai J, Zhou Y, Liu H, et al. Identification and peptidomic profiling of exosomes in preterm human milk: insights into necrotizing enterocolitis prevention. *Mol Nutr Food Res*. 2019;63(13):e1801247.
50. Miyake H, Lee C, Chusilp S, Bhalla M, Li B, Pitino M, et al. Human breast milk exosomes attenuate intestinal damage. *Pediatr Surg Int*. 2020;36(2):155–63.
51. Reinhardt TA, Lippolis JD, Nonnecke BJ, Sacco RE. Bovine milk exosome proteome. *J Proteom*. 2012;75(5):1486–92.
52. Martin CR, Dammann O, Allred EN, Patel S, O'Shea TM, Kuban KCK, et al. Neurodevelopment of extremely preterm infants who had necrotizing enterocolitis with or without late bacteremia. *J Pediatr*. 2010;157(5):751–6.e1.
53. Gussenhoven R, Westerlaken RJJ, Ophelders DRMG, Jobe AH, Kemp MW, Kallapur SG, et al. Chorioamnionitis, neuroinflammation, and injury: timing is key in the preterm ovine fetus. *J Neuroinflamm*. 2018;15(1):1–3.
54. Nino DF, Zhou Q, Yamaguchi Y, Martin LY, Wang S, Fulton WB, et al. Cognitive impairments induced by necrotizing enterocolitis can be prevented by inhibiting microglial activation in mouse brain. *Sci Transl Med*. 2018;10(471):eaan0237.
55. Gutziet O, Iluz R, Ben Asher H, Segal L, Ben Zvi D, Ginsberg Y, et al. Maternal N-acetyl-cysteine prevents neonatal hypoxia-induced brain injury in rat model. *Int J Mol Sci*. 2021;22(24):13629.
56. Paton MCB, McDonald CA, Allison BJ, Fahey MC, Jenkin G, Miller SL. Perinatal brain injury as a consequence of preterm birth and intrauterine inflammation: designing targeted stem cell therapies. *Front Neurosci*. 2017;11:200.
57. D'Aversa TG, Weidenheim KM, Berman JW. CD40-CD40L interactions induce chemokine expression by human microglia. *Am J Pathol*. 2002;160(2):559–67.
58. Putlyaeva LV, Demin DE, Korneev KV, Kasyanov AS, Tatosyan KA, Kulakovskiy IV, et al. Potential markers of autoimmune diseases, alleles rs115662534(T) and rs548231435(C), disrupt the binding of transcription factors STAT1 and EBF1 to the regulatory elements of human CD40 gene. *Biochemistry*. 2018;83(12):1534–42.
59. Smith TJ, Sciaky D, Phipps RP, Jennings TA. CD40 expression in human thyroid tissue: evidence for involvement of multiple cell types in autoimmune and neoplastic diseases. *Thyroid*. 1999;9(8):749–55.
60. Hu YC, Wang F, Zhang DD, Sun Q, Li W, Dai YX, et al. Expression of intestinal CD40 after experimental traumatic brain injury in rats. *J Surg Res*. 2013;184(2):1022–7.
61. Togo T, Akiyama H, Kondo H, Ikeda K, Kato M, Iseki E, et al. Expression of CD40 in the brain of Alzheimer's disease and other neurological diseases. *Brain Res*. 2000;885(1):117–21.
62. Becher B, Blain M, Antel JP. CD40 engagement stimulates IL-12 p70 production by human microglial cells: basis for Th1 polarization in the CNS. *J Neuroimmunol*. 2000;102(1):44–50.
63. Wu W, Alexis NE, Bromberg PA, Jaspers I, Peden DB. Mechanisms of LPS-induced CD40 expression in human peripheral blood monocytic cells. *Biochem Biophys Res Commun*. 2009;379(2):573–7.
64. Sharif O, Bolshakov VN, Raines S, Newham P, Perkins ND. Transcriptional profiling of the LPS induced NF-kappaB response in macrophages. *BMC Immunol*. 2007;8:1.
65. Liu S, Feng G, Wang GL, Liu GJ. p38MAPK inhibition attenuates LPS-induced acute lung injury involvement of NF-kappaB pathway. *Eur J Pharmacol*. 2008;584(1):159–65.
66. Wang L, Yang J-W, Lin L-T, Huang J, Wang X-R, Su X-T, et al. Acupuncture attenuates inflammation in microglia of vascular dementia rats by inhibiting miR-93-mediated TLR4/MyD88/NF-kB signaling pathway. *Oxid Med Cell Longev*. 2020;2020:1–15.
67. Zhang N, Ahsan MH, Zhu L, Sambucetti LC, Purchio AF, West DB. Regulation of Ikb $\alpha$  expression involves both NF-kB and the MAP kinase signaling pathways. *J Inflamm*. 2005;2(1):10.
68. Owen AM, Luan L, Burelbach KR, McBride MA, Stothers CL, Boykin OA, et al. MyD88-dependent signaling drives toll-like receptor-induced trained immunity in macrophages. *Front Immunol*. 2022;13:1044662.
69. Ban M, Su H, Zeng X, Chen C, Zhou S, Chen X, et al. An active fraction from *Spatholobus suberectus* dunn inhibits the inflammatory response by regulating microglia activation, switching microglia polarization from M1 to M2 and suppressing the TLR4/MyD88/NF-kappaB pathway in LPS-stimulated BV2 cells. *Heliyon*. 2023;9(4):e14979.
70. Li Q, Wang F, Wang Q, Zhang N, Zheng J, Zheng M, et al. SPOP promotes ubiquitination and degradation of MyD88 to suppress the innate immune response. *PLoS Pathog*. 2020;16(5):e1008188.
71. Lee B-C, Miyata M, Lim JH, Li J-D. Deubiquitinase CYLD acts as a negative regulator for bacterium NTHi-induced inflammation by suppressing K63-linked ubiquitination of MyD88. *Proc Natl Acad Sci*. 2016;113(2):E165–71.
72. Jin X, Shi Q, Li Q, Zhou L, Wang J, Jiang L, et al. CRL3-SPOP ubiquitin ligase complex suppresses the growth of diffuse large B-cell lymphoma by negatively regulating the MyD88/NF-kB signaling. *Leukemia*. 2020;34(5):1305–14.
73. Mathes E, O'Dea EL, Hoffmann A, Ghosh G. NF-kB dictates the degradation pathway of Ikb $\alpha$ . *EMBO J*. 2008;27(9):1357–67.
74. Darragh J, Ananieva O, Courtney A, Elcombe S, Arthur C, Simon J. MSK1 regulates the transcription of IL-1ra in response to TLR activation in macrophages. *Biochem J*. 2010;425(3):595–602.
75. Gorska MM, Liang Q, Stafford SJ, Goplen N, Dharajiya N, Guo L, et al. MK2 controls the level of negative feedback in the NF-kB pathway and is essential for vascular permeability and airway inflammation. *J Exp Med*. 2007;204(7):1637–52.
76. Zhong H, Voll RE, Ghosh S. Phosphorylation of NF-kB p65 by PKA stimulates transcriptional activity by promoting a novel bivalent interaction with the coactivator CBP/p300. *Mol Cell*. 1998;1(5):661–71.
77. Todd L, Palazzo I, Suarez L, Liu X, Volkov L, Hoang TV, et al. Reactive microglia and IL1 $\beta$ /IL-1R1-signaling mediate neuroprotection in excitotoxin-damaged mouse retina. *J Neuroinflamm*. 2019;16(1):1–9.
78. Gleeson LE, Sheedy FJ, Palsson-Mcdermott EM, Triglia D, O'Leary SM, O'Sullivan MP, et al. Cutting edge: *Mycobacterium tuberculosis* induces aerobic glycolysis in human alveolar macrophages that is required for control of intracellular bacillary replication. *J Immunol*. 2016;196(6):2444–9.
79. Hu X, Paik PK, Chen J, Yarinina A, Kockeritz L, Lu TT, et al. IFN- $\gamma$  suppresses IL-10 production and synergizes with TLR2 by regulating GSK3 and CREB/AP-1 proteins. *Immunity*. 2006;24(5):563–74.
80. Yuba E, Budina E, Katsumata K, Ishihara A, Mansurov A, Alpar AT, et al. Suppression of rheumatoid arthritis by enhanced lymph node trafficking of engineered interleukin-10 in murine models. *Arthritis Rheumatol*. 2021;73(5):769–78.
81. Schreiber S, Fedorak RN, Nielsen OH, Wild G, Williams CN, Nikolaus S, et al. Safety and efficacy of recombinant human interleukin 10 in chronic active Crohn's disease. *Gastroenterology*. 2000;119(6):1461–72.
82. Mittal SK, Cho K-J, Ishido S, Roche PA. Interleukin 10 (IL-10)-mediated Immunosuppression. *J Biol Chem*. 2015;290(45):27158–67.
83. Bretscher PA. A two-step, two-signal model for the primary activation of precursor helper T cells. *Proc Natl Acad Sci*. 1999;96(1):185–90.
84. Stoecklin G, Tenenbaum SA, Mayo T, Chittur SV, George AD, Baroni TE, et al. Genome-wide analysis identifies interleukin-10 mRNA as target of tristetraprolin. *J Biol Chem*. 2008;283(17):11689–99.
85. Gong XW, Yang QH, Yan HZ, Zhang YP, Liang YJ, Liu YZ, et al. Effects of soothing liver and invigorating spleen recipes on LPS-induced hepatocytes injury of rats and TLR4/p38MAPK signal pathway. *Zhongguo Zhong Yao Za Zhi*. 2014;39(20):4027–33.
86. Kumar RP, Abraham A. Inhibition of LPS induced pro-inflammatory responses in RAW 264.7 macrophage cells by PVP-coated naringenin

- nanoparticle via down regulation of NF-kappaB/P38MAPK mediated stress signaling. *Pharmacol Rep.* 2017;69(5):908–15.
87. Bhat NR, Zhang P, Lee JC, Hogan EL. Extracellular signal-regulated kinase and p38 subgroups of mitogen-activated protein kinases regulate inducible nitric oxide synthase and tumor necrosis factor- $\alpha$  gene expression in endotoxin-stimulated primary glial cultures. *J Neurosci.* 1998;18(5):1633–41.
88. Culbert AA, Skaper SD, Howlett DR, Evans NA, Facci L, Soden PE, et al. MAPK-activated protein kinase 2 deficiency in microglia inhibits pro-inflammatory mediator release and resultant neurotoxicity: relevance to neuroinflammation in a transgenic mouse model of Alzheimer disease. *J Biol Chem.* 2006;281(33):23658–67.
89. Crivellaro S, Panuzzo C, Carrà G, Volpengo A, Crasto F, Gottardi E, et al. Non genomic loss of function of tumor suppressors in CML: BCR-ABL promotes I $\kappa$ B $\alpha$  mediated p53 nuclear exclusion. *Oncotarget.* 2015;6(28):25217–25.

### **Publisher's Note**

Springer Nature remains neutral with regard to jurisdictional claims in published maps and institutional affiliations.